

THE ROLE OF C₂ IN NANOCRYSTALLINE DIAMOND GROWTH

J.R. Rabeau^{a*}, Y. Fan^b, P. John^a, and J.I.B. Wilson^a

a) School of Engineering and Physical Sciences, Heriot-Watt University, Edinburgh, Scotland, EH14 4AS

b) Department of Applied Physics and Electronic & Mechanical Engineering, University of Dundee, Scotland, DD1 4HN

*present address: Micro Analytical Research Centre, School of Physics, The University of Melbourne, Melbourne, Australia, 3010

E mail: jrabeau@physics.unimelb.edu.au

PACS: 81.15.Gh, 81.05.Uw, 42.62.Fi

To be published in J. Appl. Phys.

ABSTRACT

This paper presents findings from a study of nanocrystalline diamond (NCD) growth in a microwave plasma chemical vapour deposition (CVD) reactor. NCD films were grown using Ar/H₂/CH₄ and He/H₂/CH₄ gas compositions. The resulting films were characterised using Raman spectroscopy, scanning electron microscopy and atomic force microscopy. Analysis revealed an estimated grain size of the order of 50 nm, growth rates in the range 0.01 to 0.3 μm/h and *sp*³ and *sp*² bonded carbon content consistent with that expected for NCD.

The C₂ Swan band (*d* ³Π_g ↔ *a* ³Π_u) was probed using cavity ring-down spectroscopy (CRDS) to measure the absolute C₂ (*a*) number density in the plasma during diamond film growth. The number density in the Ar/H₂/CH₄ plasmas was in the range 2 to 4 x 10¹² cm⁻³, but found to be present in quantities too low to measure in the He/H₂/CH₄ plasmas. Optical emission

spectrometry (OES) was employed to determine the relative densities of the C₂ excited state (d) in the plasma.

The fact that similar NCD material was grown whether using Ar or He as the carrier gas suggests that C₂ does not play a major role in the growth of nanocrystalline diamond.

1. INTRODUCTION

In recent years, nanocrystalline diamond (NCD) has been identified as a potentially useful material for many applications such as wear-resistant coatings, MEMS and electron field emitters. NCD films are composed of diamond grains of the order of 50 nm, and under certain conditions display smooth morphology. In order to fully exploit NCD, a greater understanding of the chemical vapour deposition (CVD) growth process is essential to produce material suitable for specific applications. In particular, identification of the primary growth species would be useful for optimisation of the process parameters. Several research groups have employed spectroscopic techniques to measure the predominant species present during growth as a function of process parameters, especially under conditions of high argon concentration, typically argon/hydrogen/methane gas mixtures. Correlation between materials grown and species present in the growth environment is an important step in identifying the primary growth species.

Gruen and co-workers^{1,2,3,4,5} have been major contributors to NCD research over the past 10 years. Preliminary work² demonstrated the growth of NCD using C₆₀ in an Ar/H₂ microwave discharge. Strong C₂ Swan band optical emission was observed using OES and from this it was proposed that C₂ may be the growth species for NCD. Ab-initio calculations supported the hypothesis that C₂ could insert directly into the C-H bonds which terminate the growing diamond surface. Similar results were obtained using Ar/H₂/CH₄ gas compositions in a microwave plasma using low H₂ (<10%) and high Ar (>90%) plus a constant CH₄ proportion (~1%). However *quantitative* data on the species present in the plasma is lacking together with characterisation of resulting diamond films. Correlation in this context may elucidate precisely what processes contribute to NCD film growth.

Several non-intrusive techniques are available for studying plasma chemistry. The simplest is OES which measures the spectral emission of the plasma and provides relative populations of excited state species. OES suffers from the inability to easily calibrate excited state emission intensities with absolute concentrations in the ground state. Ar/H₂/CH₄ plasmas have been shown to produce strong C₂ Swan band emissions (C₂ d-a) at around 516 nm, giving the plasma an emerald green colour. Laser induced fluorescence (LIF) is a non-invasive spectroscopy technique which can directly probe ground state levels and has been employed widely to study CVD chemistry. LIF has the advantage of high spatial resolution combined with negligible background effects. Careful calibration with a known quantity is required however to extract absolute concentrations. Absorption spectroscopy, where the change in intensity of light is measured after passing through a sample, is the simplest way to measure absolute concentrations (Beer-Lambert law). Because the technique may involve measuring small changes in intensity of the probe beam, it is limited by the inherent fluctuations of the light source. One way to improve on this limitation is to increase the path length of the beam through the sample by, for example, using a White-cell arrangement. Goyette *et al.*⁶ used absorption spectroscopy in parallel with OES to show a correlation between the excited C₂ (d) state and the lower C₂ (a) state while changing parameters in a microwave plasma.

Cavity ring-down spectroscopy (CRDS) is a direct absorption technique which is an effective, non-invasive probe allowing high-sensitivity measurement of the absolute concentrations of species in hot filament, flame and plasma environments. Early work was done by Wahl *et al.*⁷ who used CRDS to study the methyl radical (CH₃) in a resistively heated tungsten hot-filament reactor for diamond deposition. The methyl radical may be an important precursor to diamond formation and is often considered to be the growth species in CH₄/H₂ plasmas.^{8,9} Quantitative number density spatial profiles for CH₃ were measured at

different distances from the hot-filament and at different temperatures. Further studies¹⁰ showed good agreement between experimental data and two-dimensional models of the system. Lommatzsch *et al.*¹¹ used CRDS to study the $A^2\Delta - X^2\Pi$ transition of CH at 431 nm in a diamond forming hot-filament reactor. Rotational temperature and concentration profiles were measured with respect to distance from the filament. Scherer *et al.*¹² used infrared ($3200\text{ cm}^{-1} \sim 3.1\ \mu\text{m}$) CRDS in conjunction with coherent anti-Stokes Raman spectroscopy (CARS) to determine absolute methyl radical concentrations in low pressure methane-air flames. They achieved a fractional absorption sensitivity of 3 – 10 ppm/pass. Absolute concentrations of CN, CH and CH_2O were measured using CRDS and LIF in low pressure pre-mixed flames by Luque *et al.*^{13,14}. The combination of spatially resolved LIF measurements and highly sensitive absolute number densities from CRDS produced quantitative two-dimensional images of the flame. The absolute ground state population of the methyldine radical (CH) was measured by Engeln *et al.*¹⁵ at $\sim 430\text{ nm}$ in an Ar/ C_2H_2 expanding arc plasma. The density was measured as a function of arc current and acetylene flow rate. Methyldine trends showed that it likely plays a minor role in the deposition of hydrogenated amorphous carbon.

CRDS has been used for the detection of C_2 radicals in the $A^1\Pi_u$ state and the $a^3\Pi_u$ state and most recently $X^1\Sigma_g^+$. Staicu *et al.*¹⁶ measured the absolute concentration of the $A^1\Pi_u$ state of C_2 in an atmospheric oxy-acetylene flame. The authors estimated the temperature distribution and applied the Abel inversion technique to convert the CRDS measured column densities to absolute number density profiles. Peak concentrations ranged from 8×10^{14} to $2.5 \times 10^{15}\text{ m}^{-3}$. Absolute CN radical concentrations were measured in the same oxyacetylene flame during diamond deposition. Column density measurements showed that nitrogen addition influenced mainly the central region of the flame (within a radius of $\sim 2.7\text{ mm}$). CH

was also measured¹⁷ and a correlation between local growth rate and CH concentration profiles were established. CH was concluded to play an important role in the formation of an annulus on the film, which displayed enhanced diamond growth.

Benedikt and co-workers¹⁸ studied the species C, C₂, CH, and C₂H in a remote Ar/C₂H₂ expanding thermal plasma. The C₂ (a³Π_u) radical behaviour was measured as a function of C₂H₂ flow and the a-C:H films were characterised. The plasma chemistry under these conditions was dominated by charge exchange (Ar and C₂H₂) and dissociative ion-electron recombination. The first demonstration of CRDS applied to microwave plasmas was published by John *et al.*¹⁹ who measured C₂ as a function of methane content and correlated the a³Π_u state in absorption with the d³Π_g state in emission (using OES). A linear relationship between the CRDS and OES signals was demonstrated. Wills *et al.*²⁰ measured C₂ and CH in a dc arc jet reactor. They used the spectral data in conjunction with spectral simulations to determine the rotational temperature (3300 K) and absolute number densities (6×10^{12} to 1.5×10^{13} cm⁻³) of C₂ (a³Π_u). These experiments were done under conditions favourable for diamond growth although no information was provided on the nature of the films.

The low lying C₂ (a³Π_u) electronic state is only 716 cm⁻¹ above the absolute ground state (X¹Σ_g⁺). At the temperatures expected in the plasma CVD process environment, the metastable a-state should therefore be highly populated. C₂(X) has much faster reaction rates with molecular hydrogen and hydrocarbons than C₂(a),²¹ and it was therefore thought that the C₂ (a) state would be more densely populated than C₂(X). However, it was recently shown using CRDS²² in an arc jet reactor that the C₂(X) relative to C₂(a) population is very close to that predicted by a Boltzmann distribution indicating thermal equilibrium. This result suggested a negligible depletion of C₂(X) with respect to C₂(a), or intersystem crossing

between the two states which are rapid enough to maintain thermal equilibrium and compensate for the enhanced reactivity of $C_2(X)$.

To date most NCD work has concentrated on the effects of progressively adding Ar to the growth process (whilst reducing the H_2 content). We present a study which compares separately the addition of argon and helium to the growth process, and CRDS measurements examine the absolute number density of C_2 within the plasma during NCD growth. With the addition of Ar, there was an abundance of C_2 ($\sim 10^{12} \text{ cm}^{-3}$) and with the addition of He, the quantity of C_2 was below the detection threshold of our spectrometer ($< 10^9 \text{ cm}^{-3}$).

The work presented here raises questions regarding the proposition that C_2 is the key growth species for nanocrystalline diamond. Based on the evidence obtained from experiments, with Ar and He as diluents, it appears that NCD films can be grown under conditions where the C_2 concentration is extremely small.

2. EXPERIMENTAL

A. CVD reactor

The stainless steel reactor chamber had four CF 250 ports on each side, one connected via a gate valve to a load lock. A 19 cm long and 19 cm diameter quartz cylinder with microwave shielding mesh was mounted on top of the main chamber and provided the main reaction volume. Six symmetrical CF70 ports were added via quartz extension tubes fused to the quartz cylinder. These ports were arranged axially, providing the capability for cavity ring-down spectroscopy measurements of up to three species simultaneously. The roughing and backing pump was a two stage E2M40 HV rotary pump (Edwards) and the turbomolecular pump was an EXC 300 controlled EXT 501/160 CF (Edwards). Pressure was measured using an active Pirani gauge APG-M-NW16 AL (Edwards) and a Barocel 600 capacitance

manometer (Edwards). A throttle valve model MDV-015S06 (Tylan General) and Model 80-2 controller (Vacuum General) was used to control the chamber pressure.

A coaxial blade reactor (CBR) which employed a novel microwave power applicator (DILAB Ltd) was used to grow the films discussed in this paper. The power applicator had 12 blades distributed evenly around a 19 cm diameter aluminum plate. The blades were 2.5 cm wide and extended 6 cm downwards from the bottom edge of the plate (see FIG. 1).

The microwave supply and magnetron was a Muegge model MW-GPERE 3327-5K-02, with a frequency of 2.46 GHz, 6 kW max. The microwaves were guided through a rectangular, fan cooled waveguide to the microwave applicator. The waveguide was equipped with three tuning stubs and a tuning plunger for optimal mode matching into the microwave cavity.

The 'low flow' gases (H_2 and CH_4) were controlled with Ultraflo Massflow controllers (Vacuum General) capable of 0-100 standard cubic centimetres per minute (sccm) flow rates. The 'high flow' rate gases (Ar and He) were controlled using Tylan FC2901 mass flow controllers (Millipore) capable of 0-1 standard cubic litres per minute (sclm) flow rates.

H_2 and CH_4 were premixed after the mass flow controllers (MFC) and flowed into the chamber through $\frac{1}{4}$ inch stainless steel piping and distributed around the inside perimeter chamber through a specially machined stainless steel ring with small axially spaced holes. Ar and He were fed through $\frac{1}{4}$ inch ports added to the quartz extension tubes. The high inert gas flow kept the volume within these tubes free of particulates, which drastically affected the cavity ring-down spectroscopy measurements when present.

During growth, the substrate temperature was measured in the reactor using a one-colour optical pyrometer mounted to the top of the reactor with the alignment optics focused on the silicon substrate. The emissivity of the silicon substrate was taken to be 0.62 under the estimated temperature conditions (~ 500 °C).

Optical emission spectra (OES) were collected using a PC-controlled, grating based, optical spectrum analyser (Monolite 6800). A fibre optic cable attached to a small view port on the plasma reactor guided the light to the input slit of the spectrometer.

B. Growth and Analysis

Substrates were nucleated by manually polishing an entire 4 inch wafer with 0.5 to 0.75 μm diamond powder (DeBeers Industrial Diamond). The wafer was then cut into 2 x 2 cm squares using a diamond-scriber and cleaned with acetone, methanol, Decon solution and deionised water.

Growth experiments in the CBR focused on the change of gas composition, specifically the increase of inert gas proportion (Ar or He) added to CH_4 and H_2 . Diamond films were analysed for trends in surface morphology, growth rate, diamond/graphite content and crystallite size. Raman spectroscopy, atomic force microscopy (AFM) and scanning electron microscopy (SEM) were used.

The following parameters were maintained constant for all experiments unless stated otherwise: 2.1 kW microwave power, 90 Torr (12 kPa) total pressure, 7.5 hr growth time, 480 sccm total flow. Table I summarises the substrate temperature and gas flow rates for each sample run.

Raman analysis was performed at Leeds University, UK, with a Renishaw RM1000 spectrometer with an intracavity frequency-doubled 244 nm continuous wave argon ion laser (Innova 300 FreD, Coherent Inc., Santa Clara, CA). All spectra were obtained with 1 mW laser power through a 40x objective lens.

The scanning electron microscope (SEM) was an Hitachi 2700 SEM, which detects secondary electron emission from the sample surface. The system was operated with 10 keV

electron energy. Atomic force microscope (AFM) images were collected using a Dimension 3000 Atomic Microscope (Digital Instruments, USA).

C. Cavity ring-down spectroscopy

1. CRDS theory

CRDS measures the rate of decay of a laser pulse passing back and forth through a sample contained within an optical cavity. A pulse of light is injected into a high-finesse optical cavity consisting of two axially aligned high reflectivity mirrors M1 and M2. In this instance, most of the light will be back-reflected, but a small fraction will leak into the cavity and proceed to M2. When this ‘attenuated’ pulse reaches mirror M2 within the cavity, again, most of the light will be back-reflected toward M1 and a small amount will leak out of the cavity. A detector placed on the other side of M2 to detect the fraction of light leaking out after each round-trip of the pulse within the cavity will show that the pulse intensity decays according to the Beer-Lambert law:

$$I = I_0 \exp(-t/\tau) = I_0 \exp(-kt) \quad \text{Equation (1)}$$

Where I is the initial intensity, I_0 the instantaneous intensity, k is the decay rate and τ is the time for $I = I_0/e$. The resulting decay-curve is known as a “ring-down” curve. The pulse will ring-down faster if there is an absorber in the cavity, and the spectrum of the absorber can be defined using a tuneable laser to scan the wavelength over a spectral region of interest and measuring the decay rate at different each wavelength point.

The change in the ring-down rate coefficient, Δk (off and on-resonance with a spectral feature in the cavity – in this case C_2 (a-d), is related to the absorbance, α , by the following:

$$\alpha = \frac{L\Delta k}{lc} \quad \text{Equation (2)}$$

Where L is the RD cavity mirror spacing, l is the estimated path length through the plasma and c is the speed of light. L/l accounts for the fact that the species is not homogeneous over the entire cavity length, but confined to the plasma volume. In these experiments the plasma volume was defined as the volume where emission was visible by eye and l was measured by comparing the plasma diameter with the known diameter of the substrate holder. The integrated absorption coefficient is related to the C_2 number density by the following equation:²⁰

$$\int_{line} \alpha_\nu d\nu = \frac{\lambda^2}{8\pi c} \frac{g_d}{g_a} [C_2(a)] A_{00} p \frac{1}{Q_\nu} \quad \text{Equation (3)}$$

Where, λ is the transition wavelength, $g_d = g_a = 3$ are the electronic degeneracies,²³ $[C_2(a)]$ is the number density of C_2 in the a-state over all vibrational levels, and A_{00} ($7.21 \pm 0.30 \times 10^6$ s⁻¹) is the Einstein A coefficient for the $(0,0)$ band taken from Wills *et al.*²⁰ which includes the fluorescence lifetime ($\tau = 101.8 \pm 4.2$ ns, $d^3\pi_g, v^1 = 0$) and the Franck-Condon factor ($Q_{00} = 0.7335$). The factor p is the fractional contribution of the integrated line to the total $(0,0)$ band oscillator strength at a given rotational temperature (T_{rot}). Spectral simulations and fitting were performed using PGopher^{24,25} to estimate T_{rot} and calculate the p factor. PGopher simulations include Boltzmann factors and line strengths and are thus useful for simple computation of the temperature dependent p factor. The final factor, Q_ν , is the vibrational partition function, which accounts for the Boltzmann distribution of populations in higher vibrational levels. The integrated absorption coefficient, $\alpha_\nu d\nu$, was measured by fitting a Gaussian curve to the spectral feature and determining its area.

2. CRDS experimental

The cavity ring-down spectrometer consisted of a wavelength tuneable probe laser (Continuum Surelite Nd:YAG SLI-10 pumped dye laser Sirah Laser-und Plasmatechnik

GmbH, 2400 lines/mm grating) operated with coumarin 307 radiant dye for the measurement of the C₂ Swan band (band head at 516.5 nm).

The pump laser typically ran at 10 Hz giving a frequency-tripled 355 nm output and 7 – 10 ns pulse duration. The attenuated probe beam (dye laser, 1-2 mJ after neutral density filtering) was passed through a pair of telescoping lenses, which provided a beam diameter of 2mm.

The probe laser pulses were injected into a 70 cm high-finesse optical cavity, the axis of which crossed the centre of the plasma. The mirrors were 6m radius of curvature and 2 cm in diameter with a factory reflectivity of >99.997% centred at 520 nm (Los Gatos Research). The mirrors were housed in 2.75 inch vacuum flange mounts with three external screw actuators and mounted with Viton gaskets to the vacuum chamber and protected from possible contamination by a continuous flow of argon or helium.

The beam was steered into the ring-down cavity with several silver coated mirrors (Edmund Optics, R > 99%, 450 – 1200 nm).

Light was detected at the output of the end mirror with a photomultiplier tube (Hamamatsu R955 side-on PMT, 160 – 900 nm responsivity) biased between 500 and 600 V (EG&G Ortec 456 HV power supply). The signal was sent to a LeCroy 9361 digital oscilloscope (300MHz). Background plasma emissions were blocked with a pair of long and short pass optical filters (to allow ~450 to 550 nm transmission). The ring-down curve was captured and sent via GPIB to a PC and processed with LabVIEW software (National Instruments).

3. RESULTS AND DISCUSSION

A. Plasma diagnostics

OES spectra were measured for the experimental conditions listed in Table 1. FIG. 2 shows typical OES spectra for Ar and He containing plasmas. C₂ (d) was observed in abundance

with Ar addition, but in very low levels with He addition. Conversely, hydrogen Balmer emission lines were very intense in the He plasmas, but very weak in the Ar plasmas.

CRDS was employed to measure the rotational temperature (T_{rot}) and absolute number density of C_2 by relating the ring-down coefficients for different spectral lines in the C_2 Swan band to the absolute number density according to Equation (3). The average T_{rot} for all conditions employing Ar/ H_2 / CH_4 gas mixtures was $3010 \text{ K} \pm 340 \text{ K}$ ($\pm 11\%$). This temperature was used for the calculation of the absolute number density of C_2 in the plasma. The number density was measured between 85 and 99 % Ar addition. FIG. 3 shows the change in C_2 concentration with respect to the Ar concentration. With the addition of He to the gas mixture, the C_2 concentration was unmeasurable, indicating levels below the detection threshold of the spectrometer.

B. Diamond film analysis

1. Diamond and non-diamond carbon

Raman spectra from films grown with either Ar or He dilution are shown in FIG. 4. UV Raman spectroscopy assessed the sp^3 and sp^2 bonded carbon content, which is an indication of, respectively, diamond and graphite in the material. Deconvolution of the spectra using Lorentzian fits revealed three significant peaks. One at $\sim 1333 \text{ cm}^{-1}$ was assigned to diamond²⁶ (sp^3 bonded carbon) and one slightly broader peak centred at $\sim 1595 \text{ cm}^{-1}$ was assigned to graphite (sp^2 bonded carbon, G-band).^{27,28,29} The third peak appeared between 1300 and 1350 cm^{-1} and was assigned to sp^2 bonded carbon (D-band).^{27,30} A fourth, broad curve was also included in the fit which accounted for the broad background luminescence.

A small, broad peak is apparent in some of the spectra, centred at $\sim 1440 \text{ cm}^{-1}$. This peak has been associated with nanocrystalline diamond and is thought to be due to the presence of transpoly acetylene.²⁸ Another small peak is visible in some of the spectra centred at ~ 1555

cm^{-1} . This has been assigned to sp^2 carbon.^{27,28,29,31} A typical deconvolution of the 244 nm Raman spectra is shown in FIG. 5.

FIG. 6 shows the integrated areas of the diamond and ‘graphite’ related peaks (sp^3 and sp^2 respectively) for both Ar and He dilution in the microwave plasma. The plot reveals that the sp^3 / sp^2 carbon proportion is constant up to 97% inert gas, where it increases in the Ar case and decreases in the He case. This may be attributed to the non-continuous films under these conditions, with the laser tending to sample local fluctuations in the material, not necessarily representative of the bulk properties.

Raman analysis of films grown with Ar and He dilution revealed the presence of peaks and relative intensities consistent with that expected for nanocrystalline diamond.^{28,30,31} Broadened and shifted diamond lines (1333 cm^{-1}) in all the films suggest a reduction in the grain size and high compressive stress³² from the phonon confinement model.^{26,33} This is expected to occur in nanocrystalline diamond and has been observed previously in nanocrystalline diamond films.^{26,33}

The development of a shoulder on some of the diamond lines in the 244 nm Raman spectra may be due to the D-band, which is attributed to sp^2 bonded carbon. The D-band was clearly visible after deconvolution of the UV Raman spectra. This feature was also observed in nanocrystalline films analysed by Ferrari *et al.*²⁸

2. *Growth rate*

Cross sectional SEM micrographs were taken of the deposits and the average film thickness measured. Two sample micrographs of films grown in Ar and He are shown in FIG. 7. Some films were not continuous, and in this case the thickness was determined based on the average height of the isolated deposits. The Ar grown films were uniform and continuous across the length of the substrate under all conditions except for 99% Ar. The He grown

films were continuous but rough in comparison to the Ar films and consisted mainly of large “ballas” structures.

The growth rates for these films are plotted as a function of inert gas addition in FIG. 8. The growth rate was shown to remain relatively constant over time from measurements made on films grown for 1, 3, 5 and 7.5 hours. The error in measuring the growth rates was estimated to be $\pm 10\%$. Growth rates between Ar and He films were very similar, suggesting the growth mechanism is the same with Ar and He dilution.

3. Crystallite size (AFM)

The AFM analysis yielded high resolution images and immediately revealed that the deposits were composed of clusters of tiny grains. Nanocrystalline diamond has been defined as being polycrystalline in nature consisting of diamond grains in the range 50 to 100 nm.³⁴ With respect to grain size criterion, films grown with 85 to 99% Ar and He addition are consistent with the grain size expected for NCD. AFM images are shown in FIG. 9 for Ar and He diluted films (90% only). Over the range 85 to 99% Ar and He, the grain size appeared to be uniform. The mean external grain size was estimated from the AFM images to be ~ 50 nm in the Ar films and ~ 53 nm for the He films.

4. Surface roughness

The surface roughness of the films, defined as the RMS of the distribution of “heights” for each point on the scan, was calculated from the AFM data over $10\ \mu\text{m}$ areas and is plotted in FIG. 10. There is clearly a morphological difference between He and Ar grown films, a feature which is also evident in the SEM images. The possible reasons for this are discussed later.

5. *Summary of Results*

In summary, NCD films which were very similar in sp^3 and sp^2 carbon content (assessed using Raman spectroscopy), grain size (assessed using AFM) and growth rate (assessed using SEM) were grown using two different gas mixtures: Ar or He diluted H_2/CH_4 . In the case of Ar dilution, the C_2 radical density was measured to be $\sim 10^{12} \text{ cm}^{-3}$ using CRDS and showed intense Swan band emissions in the OES spectra, whereas in the case of He dilution, the C_2 radical density was too low to measure using CRDS and showed only a small emission peak in the OES spectra.

Using He as a diluent, we expected to find similar plasma characteristics to Ar containing, particularly with respect to C_2 concentration. However, C_2 was present in quantities below the sensitivity of our cavity ring-down spectrometer (estimated to be $\sim 10^9 \text{ cm}^{-3}$) and at least a factor of 1000 less than that present in the Ar containing plasmas. This finding was confirmed by OES measurements which showed very weak emission from the C_2 (d) state. It has previously been shown using CRDS and OES that the C_2 (d) and C_2 (a) states correlate linearly as a function of plasma condition in an Ar/ H_2/CH_4 plasma.¹⁹

The fact that similar NCD films were grown both in the presence and in the absence of C_2 brings into question whether C_2 contributes significantly to the growth process.

C. Does C_2 play a role?

The abundance of C_2 in Ar containing plasmas can be attributed to the enhanced pathways available for C_2 production, arising from the presence of Ar^* in the plasma where energy transfer with C_2H_2 and/or C_2H forms C_2 .³⁵ The first excited state of He (He^*) has a higher energy (19.8 eV compared to 11.55 eV for Ar^*) which arguably implies that it will be less populated than Ar^* . Dissociation reactions with C_2H_2 and C_2H (ex. $Ar^* + C_2H_2 \rightarrow Ar + C_2 + H_2$) will therefore be minimal

The growth rates measured for films grown in this study are in general agreement with previously published results, which typically indicate a decrease in growth rate with increased addition of inert gas (> 60%).^{5,36,37,38,39} FIG. 11 presents a comparison of the findings of several studies by different research groups including our own. Zhou *et al.*⁵ analysed the growth rate as a function of Ar addition with constant 1% CH₄, a balance of H₂ and a constant 800°C substrate temperature. Yang *et al.*³⁶ carried out a similar Ar/H₂/CH₄ study with a constant temperature of 900°C. Baranauskas *et al.*^{37,38} compared growth rates with the addition of He and Ar with a constant 0.5% C₂H₅OH and a balance of H₂. They maintained a constant substrate temperature of 855 °C by increasing the filament current in their HF reactor, which may have influenced the growth rate. Han *et al.*³⁹ increased the Ar content in a 2% CH₄/H₂, 1 kW microwave plasma and grew films at 800 °C to 900 °C substrate temperature. The results from this work are also included in FIG. 11 for comparison. The plotted growth rate magnitudes shown in FIG. 11 were estimated from the published plots of growth rate versus vol% inert gas and do not necessarily indicate the precise magnitudes. With respect to C₂ content, Han *et al.*³⁹ and Zhou *et al.*⁵ reported an increase in C₂ content in the gas-phase as measured by OES.

FIG. 11 shows that the growth rate is influenced by inert gas addition and a reduction in H/C, and can often cause an increase in growth rate with ~ 0 to 50% dilution, and a decrease with 50 to 99% dilution.

Despite the general similarities in conditions and results, there is disagreement in the proposed mechanisms responsible for the trends in the growth rate:

Yang and co-workers³⁶ suggested that the initial drop in growth rate during their experiments (0 – 10% Ar) was due to the decrease in H required for the CH₃ growth mechanism.⁸ The subsequent increase in growth rate at 10% Ar was attributed to the C₂ mechanism⁴⁰ becoming

dominant. The growth rate was said to reach a maximum where the C_2 density reached a 'steady state' and then decreased because of the continued dilution of active species by Ar.

Zhou *et al.*⁵ maintained that, although C_2 continued to increase while the growth rate decreased (at >60 % Ar addition), C_2 was still the growth species. This was explained by calculations⁴¹ that show there is a pathway for diamond production via C_2 insertion that includes atomic H addition to the double bond of one ethylene-like group, and has a lower activation energy than the pathway that does not include H. The direct C_2 insertion mechanism has an activation barrier of *ca.* 2 kcal/mol.

Baranauskas *et al.*³⁸ proposed a slightly different argument, suggesting that Ar effectively diluted the radicals at the filament surface and thus increased their lifetime. The increased lifetime allowed them to travel further from the filament and may have ultimately increased their concentration at the growing substrate surface, thus increasing the growth rate.

There are obvious difficulties in establishing a consistent model which accounts for the change in growth rate as a function of conditions. Attempts have been made to establish a balance between the two most likely growth species, CH_3 and C_2 , over a range of conditions, however the arguments discussed above are complex.

FIG. 11b shows growth rates in the region 80 to 99% inert gas with the corresponding measured C_2 number density from the Ar containing plasmas superimposed. Aside from the trend of C_2 number density, which does not compliment the measured diamond growth rate, there is an obvious disparity with the He results in that the C_2 number density was too low for detection (at least 3 orders of magnitude less than in the Ar plasma).

We propose that C_2 cannot be the growth species for the formation of NCD. Firstly, because it simply is not present in quantities large enough⁴² to contribute in the case of He dilution, and secondly, because when it is present (in Ar dilution) it does not correlate with the

measured change in growth rate. The fact that the growth rates measured under both conditions are nearly identical suggests the same mechanism is at work.

The widely accepted growth species for diamond in H₂/CH₄ gas mixtures is the methyl radical, CH₃.^{8,9} This model involves surface H-abstraction reactions, insertion of CH₃ and further H-abstractions to form new diamond layers. Nanocrystalline diamond can be grown under conditions of high CH₄ containing (> 10 %) H₂/CH₄ gas mixtures.^{43,44,45,46} Hiramatsu *et al.*⁴³ reported a 50 nm grain size from diamond films grown in a microwave plasma at 55 Torr with 10% CH₄ in H₂. Incidentally, they measured a C₂ number density of $\sim 2 \times 10^{11} \text{ cm}^{-3}$ in the plasma using absorption spectroscopy. Haubner and Lux⁴⁶ refer to ‘coarse ballas’ diamond (nanocrystalline diamond clusters) grown in a hot filament reactor with 10% CH₄ in H₂. Chen and co-workers⁴⁴ found grain sizes of less than 100 nm on diamond films grown with 4 to 41% CH₄/H₂ microwave plasmas.

Whether using an inert gas diluent or pure CH₄/H₂ gas compositions, NCD seems to form in an H-depleted environment (reduction in H/C), perhaps where there is an enhanced mechanism for secondary nucleation. Evidence the fact that “ballas” or “cauliflower” diamond is often observed at the H-depleted perimeter of films grown in 1% CH₄/H₂ gas mixtures. If the CH₃ mechanism is indeed at play in our experiments, at some point the reduction in H/C would hinder the process and cause a decrease in the growth rate (from FIG. 11, this point appears to be at around 60% dilution). It is possible that the initial rise in growth rate is due to an enhancement in the mean free path of reactive species within the reactor. At ~60% dilution with inert gas (39% H₂ and 1% CH₄) the reduction in H is at such a level that H-abstracted surface sites become limited and the insertion of CH₃ radicals is inhibited. For comparison with gas mixtures used in this work, a 10% CH₄/H₂ gas mixture (such as that used by Hiramatsu *et al.*⁴³) is equivalent to 90% Ar or He, 9% H₂, 1% CH₄.

A significant feature of the films is the difference in surface morphology observed in the SEM micrographs. The Ar grown films took on a smooth morphology, while the He grown films were rough. This may be attributed to enhanced re-nucleation of the growing film in the presence of C₂, which effectively increases the uniformity over the entire surface. In the absence of enhanced re-nucleation, the He films tended to grow in large clusters, perhaps around the original Si-surface nucleation sites. The difference in surface morphology may also be attributed to the difference in mass between Ar and He. It is plausible that heavier neutral and ionic Ar continually bombards the growing surface and maintains uniform smoothness. Ar may be more effective at surface smoothing than He because of its higher mass, and may therefore be essential for the growth of smooth nanocrystalline diamond films.

4. CONCLUSIONS

Films were grown in the microwave reactor with Ar and He dilution from 85 to 99% (in a balance of H₂ and 1% CH₄). Films grown with Ar dilution revealed a uniform and smooth morphology (21 to 43 nm RMS roughness) in contrast to films grown with He dilution which revealed rough, ball-like morphology (600 to 61 nm RMS roughness). AFM analysis also revealed uniform ~ 50 nm grains in both Ar and He films.

The Ar and He grown films were very similar in carbon composition as shown by Raman spectroscopy. Raman spectra indicated the presence of NCD according to relative *sp*³ and *sp*² carbon content and spectral features associated with NCD.

The growth rates were measured over this range using cross-sectional SEM and found to be similar in magnitude (0.3 to 0.01 μm/h). The growth rate monotonically declined with increased inert gas content. The corresponding C₂ number density measured during Ar dilution reached a maximum at 95% Ar and declined with further Ar dilution.

The species, C_2 , does not appear to contribute as the growth species in the formation of nanocrystalline diamond in Ar/ H_2 / CH_4 and He/ H_2 / CH_4 containing microwave plasmas. Adding inert gas and reducing H_2 in H_2 / CH_4 gas mixtures causes a decrease the atomic H/C ratio. Similar growth mixtures can be achieved with a high CH_4 content in H_2 / CH_4 gas mixtures (>10%). Evidence for this is that similar ‘ballas’ or nanocrystalline diamond has been observed using pure H_2 / CH_4 gas mixtures.^{43,44,45,46} NCD has been shown to form independent of the presence of C_2 .

5. ACKNOWLEDGEMENTS

The authors wish to acknowledge financial support from the Engineering and Physical Sciences Research Council (Technological Plasmas Initiative) UK. The authors would like to thank Dr. Alastair Smith and Inigo Mendieta at the University of Leeds for the Raman analysis. J.R.R. wishes to thank Dr. Andrew Orr-Ewing and Dr. Jonathon Wills of the University of Bristol for their introductory guidance with practical aspects of CRDS and supplying a copy of PGOPHER for C_2 spectral simulations

References

- ¹ D. Zhou, A.R. Krauss, L.C. Qin, and D.M. Gruen, *J. Appl. Phys.*, 82, 4547 (1997).
- ² D.M. Gruen, S. Liu, A.R. Krauss, and X. Pan, *J. Appl. Phys.*, 75, 1758 (1994).
- ³ D.M. Gruen, S.Liu, A.R. Krauss, J. Luo, and X. Pan, *Appl. Phys. Lett.*, 64, 1502 (1994).
- ⁴ D. Zhou, T.G. McCauley, L.C. Qin, A.R. Krauss, and D.M. Gruen, *J. Appl. Phys.*, 83, 540 (1998).
- ⁵ D. Zhou, D.M. Gruen, L.C. Qin, T.G. McCauley, and A.R. Krauss, *J. Appl. Phys.*, 84, 1981 (1998).
- ⁶ A.N. Goyette, J.E. Lawler, L.W. Anderson, D.M. Gruen, T.G. McCauley, D. Zhou, and A.R. Krauss, *J. Phys. D: Appl. Phys.*, 31, 1975 (1998).

-
- ⁷ E.H. Wahl, T.G. Owana, C.H. Kruger, P. Zalicki, Y. Ma, and R.N. Zare, *Diamond Relat. Mater.*, **5**, 373 (1996).
- ⁸ S.J. Harris, *Appl. Phys. Lett.*, **56**, 2298 (1990).
- ⁹ D.G. Goodwin and J.E. Butler, in: M.A. Prelas, G. Popovici, and L.K. Bigelow (Eds.), *Handbook of Industrial Diamonds and Diamond Films*, Marcel Dekker, New York, 1998, p. 527.
- ¹⁰ E.H. Wahl, T.G. Owana, C.H. Kruger, Y. Ma, P. Zalicki, and R.N. Zare, *Diamond Relat. Mater.*, **6**, 476 (1997).
- ¹¹ U. Lommatzsch, E.H. Wahl, T.G. Owana, C.H. Kruger, and R.N. Zare, *Chem. Phys. Lett.*, **320**, 339 (2000).
- ¹² J.J. Scherer, K.W. Aniolek, N.P. Cernansky, and D.J. Rakestraw, *J. Chem. Phys.*, **107**, 16 (1997).
- ¹³ J. Luque, J.B. Jeffries, G.P. Smith, and D.R. Crosley, *Combustion and Flame*, **126**, 1725 (2001).
- ¹⁴ J. Luque, J.B. Jeffries, G.P. Smith, and D.R. Crosley., *Appl. Phys. B*, **73**, 731 (2001).
- ¹⁵ R. Engeln, K.G.Y. Letourneur, M.G.H. Boogaarts, M.C.M. van de Sanden, and D.C. Schram, *Chem. Phys. Lett.*, **310**, 405 (1999).
- ¹⁶ A. Staicu, R.L. Stolk, and J.J. ter Meulen, *J. Appl. Phys.*, **91**, 969 (2002).
- ¹⁷ R.L. Stolk and J.J. ter Meulen, *Diamond Relat. Mater.*, **8**, 1251 (1999).
- ¹⁸ J. Benedikt, K.G.Y. Letourneur, M. Wisse, D.C. Schram, and M.C.M. van de Sanden, *Diamond Relat. Mater.*, **11**, 989 (2002).
- ¹⁹ P. John, J.R. Rabeau, and J.I.B. Wilson, *Diamond Relat. Mater.*, **11**, 608 (2002).
- ²⁰ J.B. Wills, J.A. Smith, W.E. Boxford, J.M.F. Elks, M.N.R. Ashfold, and A.J. Orr-Ewing, *J. Appl. Phys.*, **92**, 4213 (2002).
- ²¹ H. Reisler, M.S. Mangir, and C. Wittig, *J. Chem. Phys.*, **73**, 2280 (1980).
- ²² C.J. Rennick, J.A. Smith, M.N.R. Ashfold, and A.J. Orr-Ewing, *Chem. Phys. Lett.*, **383**, 518 (2004).

-
- ²³ L. Brewer and L. Hagan, *High Temp. Sci.*, 11, 233 (1979).
- ²⁴ PGOPHER spectral simulation software written by C.M. Western, University of Bristol (1996).
- ²⁵ M.E. Green and C.M. Western, *J. Chem. Phys.*, 110, 385 (1999) a summary of the PGopher program.
- ²⁶ D.S. Knight and W.B. White, *J. Mater. Res.* 4, 385 (1989).
- ²⁷ A.C. Ferrari and J. Robertson, *Phys. Rev. B.* 64, 075414 (2001).
- ²⁸ A.C. Ferrari and J. Robertson, *Phys. Rev. B.* 63, 121405(R) (2001).
- ²⁹ R.J. Nemanich, J.T. Glass, G. Lucovsky, and R.E. Shroder, *J. Vac. Sci. Technol.*, A, 6, 1783 (1988).
- ³⁰ S. Buhlmann, E. Blank, R. Haubner, and B. Lux, *Diamond Relat. Mater.*, 8, 194 (1999).
- ³¹ Z. Sun, J.R. Shi, B.K. Tay, and S.P. Lau, *Diamond Relat. Mater.* 9, 1979 (2000).
- ³² L.C. Nistor, J. Van Landuyt, V.G. Ralchenko, E.D. Obraztsova, and A.A. Smolin, *Diamond Relat. Mater.*, 6, 159 (1997).
- ³³ S. Praver, K.W. Nugent, D.N. Jamieson, J.O. Orwa, L.A. Bursill, and J.L. Peng, *Chem. Phys. Lett.* 332, 93 (2000).
- ³⁴ A.R. Krauss, O. Auciello, D.M. Gruen, A. Jayatissa, A. Sumant, J. Tucek, D.C. Mancini, N. Moldovan, A. Erdemir, D. Ersoy, M.N. Gardos, H.G. Busmann, E.M. Meyer, and M.Q. Ding, *Diamond Relat. Mater.*, 10, 1952 (2001).
- ³⁵ C. Riccardi, R. Barni, M. Fontanesi, and P. Tosi, *Chem. Phys. Lett.*, 329, 66 (2000).
- ³⁶ T.-S. Yang, J.-Y. Lan, C.-L. Cheng, and M.-S. Wong, *Diamond Relat. Mater.* 10, 2161 (2001).
- ³⁷ V. Baranauskas, H.J. Ceragioli, A.C. Peterlevitz, M.C. Tosin, and S.F. Durant, *Thin Solid Films*, 377-378, 182 (2000).
- ³⁸ V. Baranauskas, H.J. Ceragioli, A.C. Peterlevitz, M.C. Tosin, and S.F. Durant, *Thin Solid Films*, 377-378, 303 (2000).
- ³⁹ Y.-S. Han, Y.-K. Kim and J.-Y. Lee, *Thin Solid Films*, 310, 39 (1997).

-
- ⁴⁰ T.G. McCauley, D.M. Gruen, and A.R. Krauss, *Appl. Phys. Lett.* 73, 1646 (1998).
- ⁴¹ P.C. Redfern, D.A. Horner, L.A. Curtiss, and D.M. Gruen, *J. Phys. Chem.*, 100, 11654 (1996).
- ⁴² J. Luque, W. Juchmann, and J.B. Jeffries, *J. Appl. Phys.*, 82, 2072 (1997).
- ⁴³ M. Hiramatsu, C.H. Lau, A. Bennett, and J.S. Foord, *Thin Solid Films*, 407, 18 (2002).
- ⁴⁴ L.C. Chen, P.D. Kichambare, K.H. Chen, J.-J. Wu, J.R. Yang, and S.T. Lin, *J. Appl. Phys.*, 89, 753 (2001).
- ⁴⁵ H. Yoshikawa, C. Morel, and Y. Koga, *Diamond Relat. Mater.*, 10, 1588 (2001).
- ⁴⁶ R. Haubner and B. Lux, *Int. J. Refr. Metals and Hard Mater.*, 20, 93 (2002).

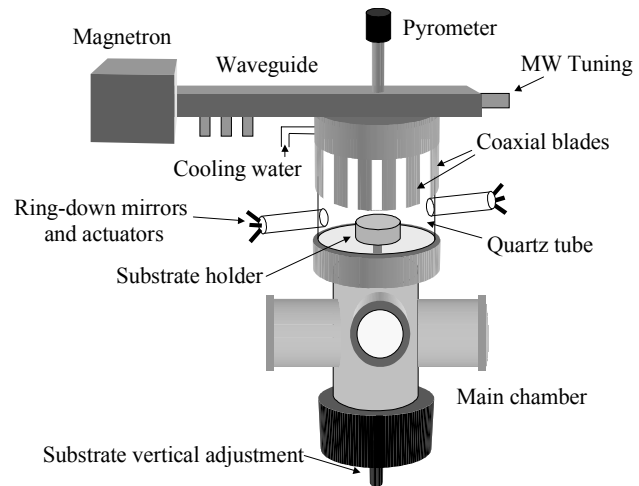
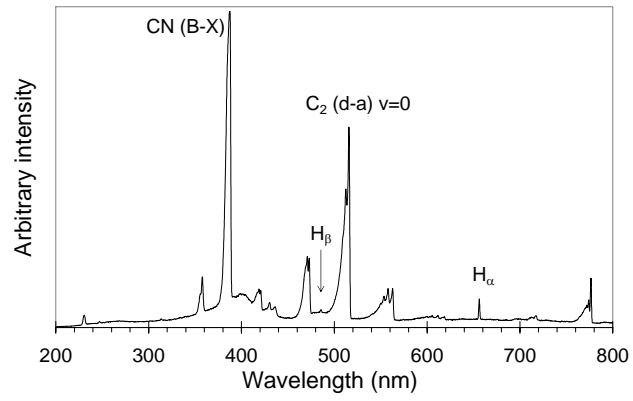


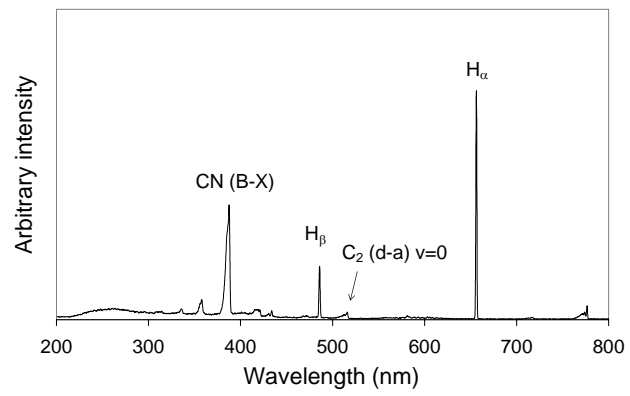
FIG. 1. J.R. Rabeau

	Sample	Ar/He (%)	H₂ (%)	CH₄ (%)	T_{substrate} (°C)
Ar	6-016	85	14	1	515
	6-015	90	9	1	450
	6-010	95	4	1	450
	6-019	97	2	1	420
	6-020	99	0	1	400
He	6-027	85	14	1	495
	6-029	90	9	1	~ 400 - 500
	6-028	95	4	1	~ 400 - 500
	6-030	97	2	1	~ 400 - 500
	6-031	99	0	1	~ 400 - 500

TABLE I. J.R. Rabeau



(a)



(b)

FIG. 2. J.R. Rabeau

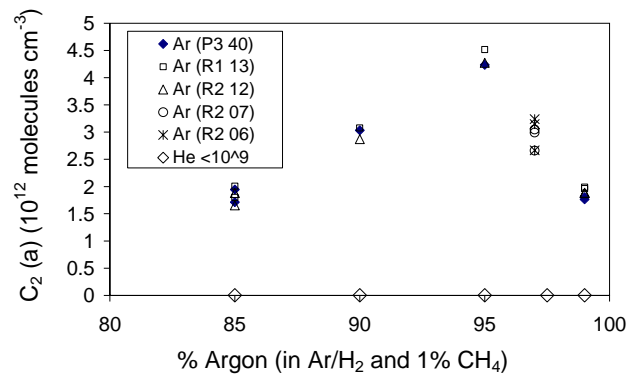


FIG. 3. J.R. Rabeau

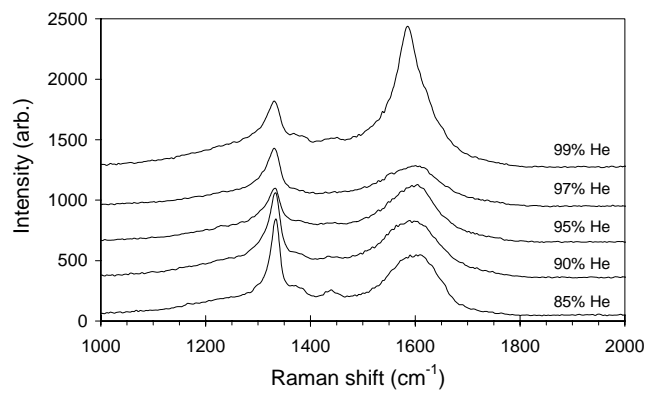
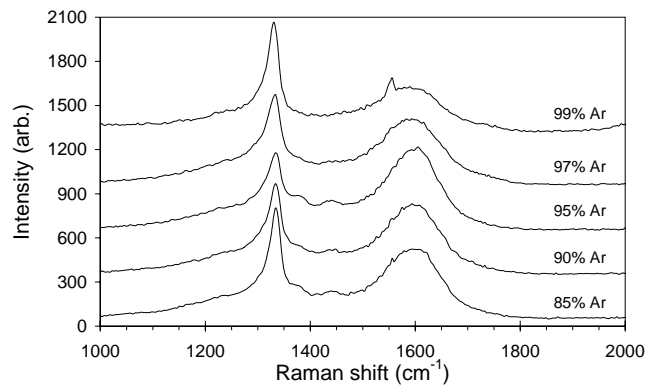


FIG. 4. J.R. Rabeau

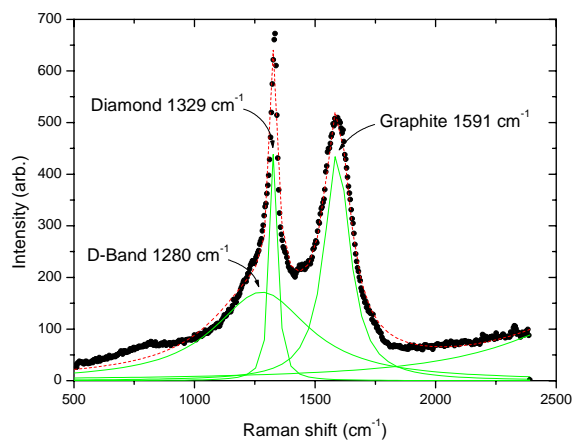


FIG. 5. J.R. Rabeau

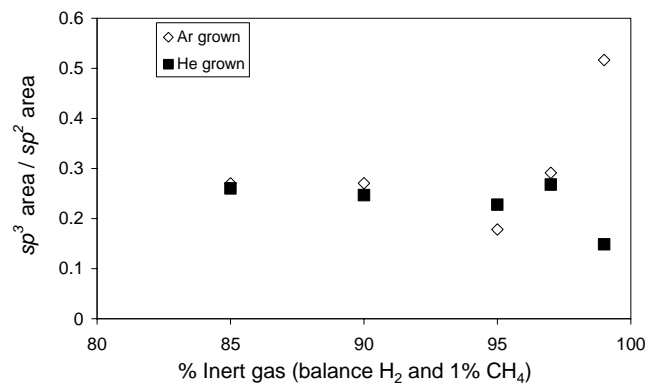


FIG. 6. J.R. Rabeau

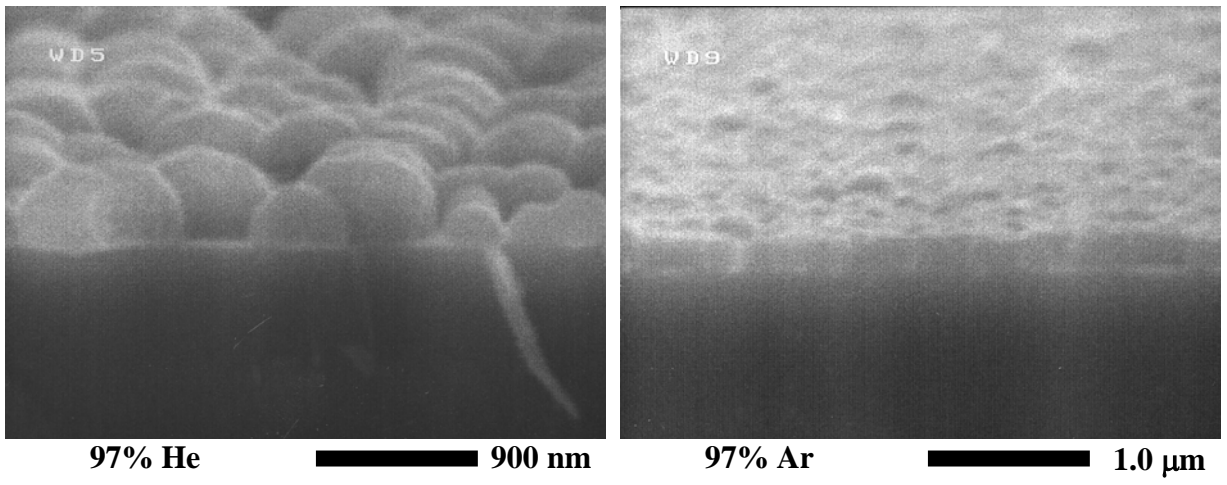


FIG. 7. J.R. Rabeau

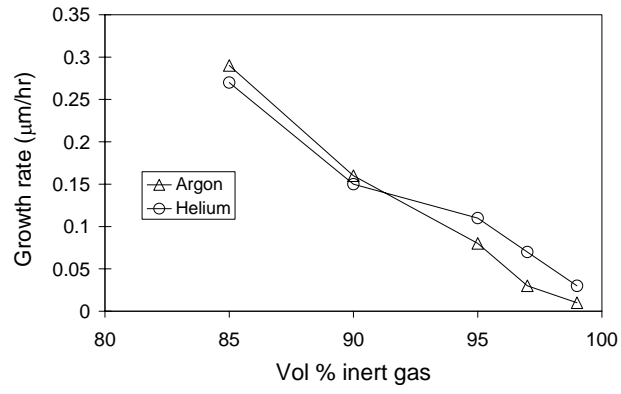
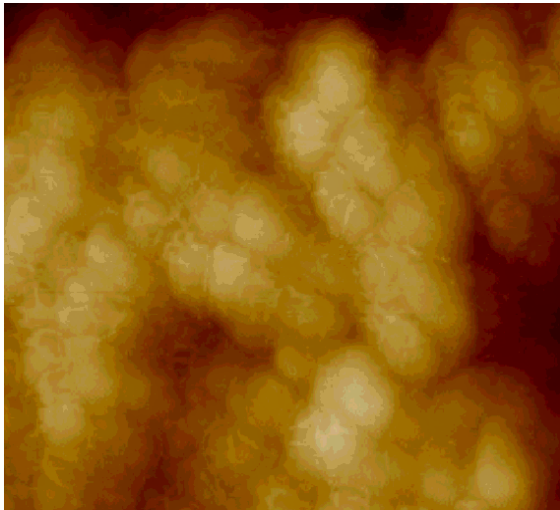
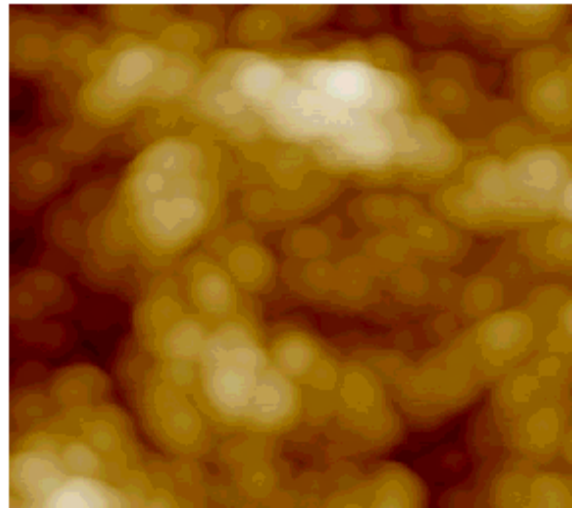


FIG. 8. J.R. Rabeau



He 250 nm



Ar 250 nm

FIG. 9. J.R. Rabeau

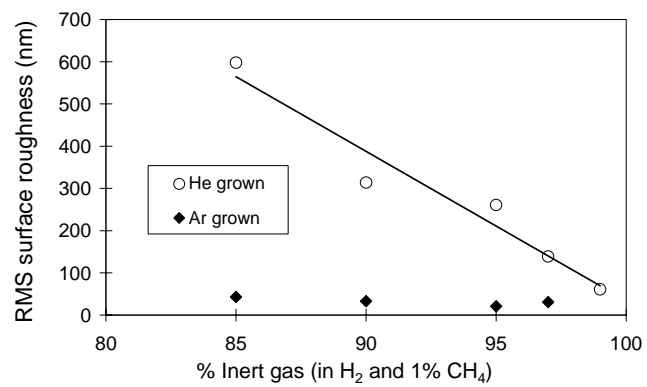


FIG. 10. J.R. Rabeau

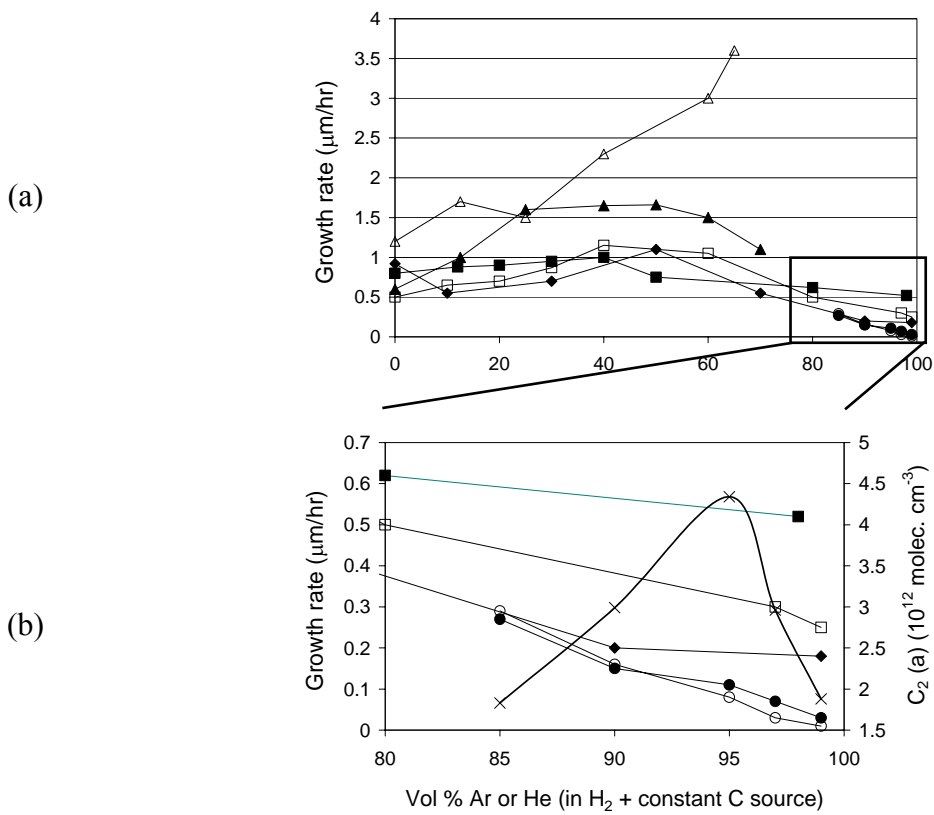


FIG. 11. J.R. Rabeau

List of Figures

FIG. 1. Coaxial blade reactor (showing only 2 of 6 diagnostic ports).

TABLE I. Growth conditions used in the CBR for growth of films with Ar and He.

FIG. 2. Typical OES spectra from (a) Ar/H₂/CH₄ and (b) He/ H₂/CH₄ plasmas in the coaxial blade reactor.

FIG. 3. C₂ (a) number density as a function of Ar content (1% CH₄ and a balance of H₂, 400 sccm total flow) in the CBR reactor at 2.1 kW and 90 Torr. The number density was measured using different spectral lines indicated by different symbols. The upper limit of C₂ (a) in the He containing plasmas is shown along the baseline of the plot.

FIG. 4. Raman spectra (244 nm) of samples grown with an increasing amount of Ar or He diluted H₂/CH₄ process gas compositions.

FIG. 5. Four Lorentzian curves (-) were fitted to the 97% Ar experimental Raman spectrum (•). The fit gave excellent agreement with the experimental data.

FIG. 6. Plot of the ratio of the diamond peak area to the ‘graphite’ peak area versus inert gas content for samples grown with an increasing amount of Ar or He diluted H₂/CH₄ process gas compositions.

FIG. 7. SEM micrographs of films grown with 97% Ar or He diluted H₂/CH₄ process gas compositions for 7.5 hours.

FIG. 8. The average growth rate of diamond films grown with an increasing amount of Ar or He diluted H₂/CH₄ process gas compositions. The error was estimated to be approximately 10%.

FIG. 9. AFM images of diamond films grown with 97% Ar or He diluted H₂/CH₄ process gas compositions for 7.5 hours.

FIG. 10. RMS roughness for films grown with an increasing amount of Ar or He diluted H₂/CH₄ process gas compositions.

FIG. 11. (a) Observed growth rates as a function of inert gas content (balance H₂ and constant CH₄ or C₂H₅OH content) taken from the literature. ◆Yang *et al.*³⁶ Ar (900°C), □Zhou *et al.*⁵ Ar (800°C), ΔBaranauskas *et al.*³⁸ Ar (855°C), ▲Baranauskas *et al.*³⁷ He

(855°C), ■ Han *et al.*³⁹ Ar (800 – 900°C), ○ This work Ar (400 – 500°C), ● This work He (< 500°C). (b) shows a magnified portion of the plot and the C₂ number density measured in our experiments during Ar addition is superimposed for comparison.